Optical phonons coupled to a Kitaev spin liquid

A. Metavitsiadis,[1,*] W. Natori,[2,3,†] J. Knolle,[4,5,2,‡] and W. Brenig[1,§]

[1]*Institute for Theoretical Physics, Technical University Braunschweig, D-38106 Braunschweig, Germany*

[2]*Blackett Laboratory, Imperial College London, London SW7 2AZ, United Kingdom*

[3]*Institut Laue-Langevin, BP 156, 41 Avenue des Martyrs, 38042 Grenoble Cedex 9, France*

[4]*Department of Physics TQM, Technical University of Munich, 85748 Garching, Germany*

[5]*Munich Center for Quantum Science and Technology (MCQST), Schellingstrasse 4, D-80799 München, Germany*

(Received 1 April 2021; revised 1 February 2022; accepted 7 April 2022; published 28 April 2022)

Emergent excitation continua in frustrated magnets are a fingerprint of fractionalization, characteristic of quantum spin-liquid states. Recent evidence from Raman scattering for a coupling between such continua and lattice degrees of freedom in putative Kitaev magnets may provide insight into the nature of the fractionalized quasiparticles. Here we study the renormalization of optical phonons coupled to the underlying $\mathbb{Z}_2$ quantum spin liquid. We show that phonon line shapes acquire an asymmetry, observable in light scattering and originating from two distinct sources, namely, the dispersion of the Majorana continuum and the Fano effect. Moreover, we find that the phonon lifetimes increase with increasing temperature due to thermal blocking of the available phase space. Finally, in contrast to low-energy probes, optical phonon renormalization is rather insensitive to thermally excited gauge fluxes and barely susceptible to external magnetic fields.

DOI: 10.1103/PhysRevB.105.165151

I. INTRODUCTION

There is an ongoing pursuit of the signatures of the elusive quantum spin-liquid (QSL) state of matter [1–3]. The difficulty to identify such states is due to the fact that they do not break any symmetries and lack conventional local order parameters of magnetic or related nature down to zero temperature. Recently, QSLs with a $\mathbb{Z}_2$ gauge structure may have actually come close to material realization, motivated by the exact solution of the famous Kitaev spin model (KSM) with compass exchange on the two-dimensional (2D) honeycomb lattice [4]. In this model, spins fractionalize into static $\mathbb{Z}_2$ gauge fluxes and itinerant Majorana fermions, with a gapless QSL ground state. In external magnetic fields the KSM opens a gap and displays chiral Majorana edge modes. Variants and generalizations of the KSM in 1D [5–11], 2D [12], and 3D [13–15], as well as for spins larger than 1/2 [16–18], have been considered.

Mott insulators with strong spin-orbit coupling (SOC) are promising materials to realize the KSM [19–22]. However, residual non-Kitaev exchange interactions remain an issue, with all current systems under consideration eventually displaying magnetic order at low temperatures. From a present perspective [3,23–26], α-$RuCl_3$, either above its ordering temperature or with magnetic order suppressed by external magnetic fields, is one of the prime candidates under scrutiny for $\mathbb{Z}_2$ QSL physics. Recent thermal Hall effect measurements in α-$RuCl_3$ suggest half-integer quantization plateaus [27] which are consistent with Majorana edge states, including a field-angular variation of the topological Chern number identical to that of the Kitaev QSL [28] and a bulk-boundary correspondence claimed in specific heat measurements [29]. In addition to edge transport, a multitude of bulk spectroscopic probes have been invoked, aiming to identify continua characteristic of the fractional Majorana excitations. This pertains to inelastic neutron scattering [30–35] and local resonance techniques [36,37], as well as to magnetic Raman scattering [38–40].

An interesting open question is whether the coupling of Majorana fermions of the putative KSM to other degrees of freedom can be used to provide signatures of their existence. Coupling to phonons [41–44] can induce characteristic renormalizations, examples of which seem to have been observed recently for acoustic phonons [45]. Regarding optical phonons, Raman scattering [46–51] has provided early on evidence for Raman active phonons with Fano line shapes, overlapping with the magnetic Raman continuum [38,39]. This has been speculated to be a signature of renormalization of optical phonons by Majorana fermions but up to now a microscopic description was missing.

Here, we provide a theory of optical phonons coupled to a KSM. We describe the microscopic details of the coupling and evaluate the phonon self-energy. The phonon renormalization versus energy and temperature is studied, the relative importance of Majorana and flux excitations is discussed, and the implications for Raman scattering are clarified. We find convincing qualitative agreement with experimental data, which points to an intriguing interpretation of a Majorana-scattering-induced optical phonon renormalization in the candidate material α-$RuCl_3$.

The paper is organized as follows. In Sec. II we develop our theory of mixing between optical phonons and Majorana

*a.metavitsiadis@tu-bs.de
†w.natori@imperial.ac.uk
‡j.knolle@tum.de
§w.brenig@tu-bs.de

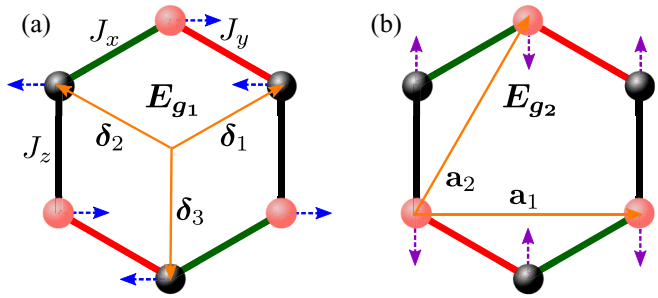

FIG. 1. Kitaev hexagons with compass magnetic interactions $J_{x,y,z}$ along the directions $\boldsymbol{\delta}_1 = \frac{a}{2}(+\sqrt{3}\boldsymbol{e}_x + \boldsymbol{e}_y)$, $\boldsymbol{\delta}_2 = \frac{a}{2}(-\sqrt{3}\boldsymbol{e}_x + \boldsymbol{e}_y)$, and $\boldsymbol{\delta}_3 = -a\boldsymbol{e}_y$, respectively. In addition the lattice vectors of the triangular Bravais lattice are shown as $\mathbf{a}_1 = a\sqrt{3}\boldsymbol{e}_x$ and $\mathbf{a}_2 = \frac{a\sqrt{3}}{2}(\boldsymbol{e}_x + \sqrt{3}\boldsymbol{e}_y)$. The distortion of the lattice due to the two optical modes $E_{g_1}(a)$ and $E_{g_2}(b)$ is indicated by the small blue and purple arrows, respectively, with a dashed shaft.

fermions. In Sec. III we evaluate and discuss the phonon self-energy, both at low and at elevated temperatures. Section IV details the resulting phonon spectra. In Sec. V, the Raman response is analyzed. Several technical details are presented in Appendices A–D.

II. OPTICAL-PHONON MAJORANA MIXING

Here, we consider phonons of a 2D Honeycomb lattice coupled magnetoelastically to the Kitaev QSL. The total Hamiltonian of the system reads $H = H_P + H_K + H_{KP}$, where H_P stands for the quadratic free phonon contribution $H_P = \sum_{\mathbf{q}m}(\omega_{m\mathbf{q}} + \frac{1}{2})b^\dagger_{m\mathbf{q}}b_{m\mathbf{q}}$, with $b^\dagger_{m\mathbf{q}}$ and $b_{m\mathbf{q}}$ being bosonic creation and annihilation operators, respectively, at momentum $\mathbf{q}$ for the mode m, and $\omega_{m\mathbf{q}}$ being the corresponding energy.

The magnetic degrees of freedom are described by the Kitaev spin Hamiltonian $H_K = \sum_{\mathbf{r},\boldsymbol{\delta}} J_{\boldsymbol{\delta}} S^{d_{\boldsymbol{\delta}}}_{\mathbf{r}} S^{d_{\boldsymbol{\delta}}}_{\mathbf{r}-\boldsymbol{\delta}}$, [4] (see also Fig. 1). Here, $\mathbf{r} = l_1\mathbf{a}_1 + l_2\mathbf{a}_2$, with $l_{1,2} = 0, 1, \ldots, L-1$, refers to a triangular Bravais lattice of linear dimension L, and $\boldsymbol{\delta}$ sets the location of the basis of the honeycomb lattice, with $N = L^2$ unit cells and $2N$ sites. The components $d_{\boldsymbol{\delta}}$ of the spin-1/2 operators S assume the values $d_{\boldsymbol{\delta}} = x$, y, and z depending on the $\boldsymbol{\delta}$ vector, while $J_{\boldsymbol{\delta}}$ are the Kitaev interactions. We consider the isotropic case $J_{\boldsymbol{\delta}} = J$ and set $\hbar$, $k_B = 1$.

Following the literature [4,6], we map the spin model onto one of two species of Majorana fermions, c and $\bar{c}$, with $\{c_i, c_j\} = 2\delta_{ij} = \{\bar{c}_i, \bar{c}_j\}$ and $\{c_i, \bar{c}_j\} = 0$. This mapping renders Majorana fermions of, e.g., c-type itinerant, while the other type pairs into static $\mathbb{Z}_2$ gauge fields $\eta = \pm 1$ along, e.g., the $\boldsymbol{\delta}_3$ direction. The gauge field generates a conserved flux, equivalent to a macroscopic number of conserved local operators in the spin language [4,52]. In the Majorana representation, H_K reads

$$H_K = J\sum_{\mathbf{r},\boldsymbol{\delta}} h_{\boldsymbol{\delta}}(\mathbf{r}), \quad h_{\boldsymbol{\delta}}(\mathbf{r}) = -\frac{i}{4}\eta_{\boldsymbol{\delta}}(\mathbf{r})c_{\mathbf{r}}\tilde{c}_{\mathbf{r}-\boldsymbol{\delta}}, \tag{1}$$

where the gauge field $\eta_{\boldsymbol{\delta}}$ acquires the values $\eta_{\boldsymbol{\delta}_1}(\mathbf{r}) = \eta_{\boldsymbol{\delta}_2}(\mathbf{r}) = 1$ and $\eta_{\boldsymbol{\delta}_3}(\mathbf{r}) = \pm 1$. Operators with a tilde reside on the basis sites. The ground state resides within the uniform gauge sector, which is separated from other sectors by a gap of $\Delta \approx 0.065J$. At finite temperature T fluxes become thermally excited and proliferate in a narrow range near a very low $T^* \approx 0.012J$. For several observables the emergent disorder introduced by the visons has been shown to be of physical significance [8,43,53,54]. For the present case of interest, i.e., optical phonons, we show that gauge excitations imply only negligible quantitative modifications.

We focus on magnetoelastic coupling between spins and lattice degrees of freedom, i.e., on the leading-order variation $J(\mathbf{u}_{\mathbf{r}} - \tilde{\mathbf{u}}_{\mathbf{r}-\boldsymbol{\delta}}) \approx J + \nabla J \cdot (\mathbf{u}_{\mathbf{r}} - \tilde{\mathbf{u}}_{\mathbf{r}-\boldsymbol{\delta}})$ of the exchange with respect to lattice deformations $\mathbf{u}_{\mathbf{r}}$ at site $\mathbf{r}$. The lattice distortions in Fourier space, $\mathbf{u}_{\mathbf{q}} = \frac{1}{\sqrt{N}}\sum_{\mathbf{r}} e^{i\mathbf{q}\cdot\mathbf{r}}\mathbf{u}_{\mathbf{r}}$, are quantized as usual in terms of phonon normal modes with $\mathcal{B}_{m\mathbf{q}} = b_{m\mathbf{q}} + b^\dagger_{m,-\mathbf{q}}$ comprising the annihilation and creation operators of mode m at momentum $\pm\mathbf{q}$ and energy $\omega_{m\mathbf{q}}$ Using this, the Majorana phonon coupling reads

$$H_{KP} = \sum_{m\mathbf{q}} \mathcal{B}_{m\mathbf{q}}\mathcal{H}_{m,-\mathbf{q}}, \quad \mathcal{H}_{m\mathbf{q}} = \sum_{\boldsymbol{\delta}} \Lambda^{\boldsymbol{\delta}}_{m\mathbf{q}} h_{\boldsymbol{\delta};\mathbf{q}}, \tag{2}$$

where the form factor of the coupling is encoded in $\Lambda^{\boldsymbol{\delta}}_{m\mathbf{q}}$ (see Appendix A for details) and $h_{\boldsymbol{\delta};\mathbf{q}} = \frac{1}{\sqrt{N}}\sum_{\mathbf{r}} e^{i\mathbf{q}\cdot\mathbf{r}} h_{\boldsymbol{\delta}}(\mathbf{r})$.

Here, we focus on the E_{g_1} and E_{g_2} optical modes observed in Raman experiments. These are of particular interest since, allegedly, they overlap with the Majorana continuum. For Raman scattering it is safe to consider $q \to 0$ only and we drop all $\mathbf{q}$ labels hereafter. In Appendix A we treat also $q \neq 0$, and moreover we treat weak magnetic fields in Appendix C. The phonon energies are $\omega_1 \equiv \omega_{g_1} \approx 116\ \mathrm{cm}^{-1} \approx 1.9J$ and $\omega_2 \equiv \omega_{g_2} \approx 165\ \mathrm{cm}^{-1} \approx 2.6J$, where we assume a Kitaev coupling of $J \approx 90$ K. The vibrational pattern of the two modes [47] is shown in Fig. 1. In terms of Eq. (2) the lattice modulations imply $\boldsymbol{\Lambda}_m = \Lambda_m[1, -1^m, \lambda_m]$, with $m = 1$ and 2, and λ_m denotes a possible anisotropy between the $\boldsymbol{\delta}_{1,2}$ and $\boldsymbol{\delta}_3$ directions. The magnitude of Λ_m can be assumed to be in the perturbative regime [43]. For additional information, a detailed microscopic derivation of the spin-phonon coupling including the effect of spin-orbit effects beyond the pure Kitaev model is given in the Supplemental Material [55]; see also Refs. [56–58].

The coupling of the phonons to the fractionalized magnetic excitations, Eq. (2), induces a renormalization to the phonon propagators $D_{mm'}(\tau) = \langle \mathcal{T}_\tau \mathcal{B}_m(\tau)\mathcal{B}^\dagger_{m'}\rangle \equiv \langle\langle \mathcal{B}_m; \mathcal{B}^\dagger_{m'}\rangle\rangle(\tau)$, with time ordering $\mathcal{T}$ and the double brackets used as shorthand (see Appendix A). In frequency space the corresponding 2×2 Dyson equation reads

$$\mathbf{D}(z) \approx \left[\mathbf{D}_0^{-1}(z) - \boldsymbol{\Sigma}(z)\right]^{-1}, \quad \boldsymbol{\Sigma}_{mm'} = \langle\langle \mathcal{H}_m; \mathcal{H}^\dagger_{m'}\rangle\rangle. \tag{3}$$

Here, z corresponds to the analytic continuation $i\omega_n \to z = \omega + i0^+$ of the Matsubara frequencies. $\mathbf{D}_0(z)$ comprises the bare phonon propagators $D^0_m(z)$, with $[\mathbf{D}_0(z)]_{mm'} = \delta_{mm'}D^0_m(z)$ and $D^0_m(z) = 2\omega_m/(z^2 - \omega_m^2)$.

The 2×2 matrix $\boldsymbol{\Sigma}(z)$ in Eq. (3) is the self-energy. A central goal of the paper is to evaluate this self-energy. We do this to leading order in the Majorana-phonon coupling and in two ways: first, analytically, assuming a uniform gauge field configuration in Eq. (1), and second, numerically, by considering a numerical random averaging over disordered configurations of the gauge field η. While the former approach is justified for $T \lesssim T^*$, the latter applies to $T \gtrsim T^*$ [43,53,54].

III. PHONON SELF-ENERGY

A. Uniform gauge

At low temperatures, $T \lesssim T^*$, it can be assumed, that the system acquires a uniform gauge configuration, $\eta_\delta = 1$, allowing for the analytical calculation of the phonon self-energy. First, the Kitaev terms in Eq. (1) can be brought to a diagonal form by going to the reciprocal space $\mathbf{k} = k_1\mathbf{G}_1 + k_2\mathbf{G}_2$, where $\mathbf{G}_1 = \frac{1}{3a}(\sqrt{3}\boldsymbol{e}_x - \boldsymbol{e}_y)$ and $\mathbf{G}_2 = \frac{2}{3a}\boldsymbol{e}_y$ are the reciprocal lattice vectors, i.e., $\mathbf{a}_i \cdot \mathbf{G}_j = \delta_{i,j}$ for $i(j) = 1$ and 2. The coefficients $k_{1,2}$ are set to antiperiodic boundary conditions $k_j = 2\pi(l_j + \frac{1}{2})/L$, to allow all Majoranas to pair into complex fermions. The Fourier transform of the Majoranas reads $c_\mathbf{k} = \sum_\mathbf{r} e^{-i\mathbf{k}\cdot\mathbf{r}} c_\mathbf{r}/\sqrt{2N}$, such that $\{c_\mathbf{k}, c^\dagger_{\mathbf{k}'}\} = \delta_{\mathbf{k},\mathbf{k}'}$, and similarly for the $\tilde{c}$ operators.

In the diagonal complex fermion basis, $\Psi^\dagger_\mathbf{k} = (d^\dagger_{1,\mathbf{k}}, d^\dagger_{2,\mathbf{k}})$, H_K and $\mathcal{H}_m$ of Eqs. (1) and (2) read $H_K = \frac{1}{2}\sum_\mathbf{k} \Psi^\dagger_\mathbf{k} E_\mathbf{k} \Psi_\mathbf{k}$ and $\mathcal{H}_m = \frac{1}{2}\sum_\mathbf{k} \Psi^\dagger_\mathbf{k} V_{m;\mathbf{k}} \Psi_\mathbf{k}$, with

$$E_\mathbf{k} = \begin{pmatrix} \epsilon_\mathbf{k} & 0 \\ 0 & -\epsilon_\mathbf{k} \end{pmatrix}, \quad V_{m;\mathbf{k}} = \begin{pmatrix} g'_{m;\mathbf{k}} & ig''_{m;\mathbf{k}} \\ -ig''_{m;\mathbf{k}} & -g'_{m;\mathbf{k}} \end{pmatrix}. \tag{4}$$

The energy eigenvalues are given by $\epsilon_\mathbf{k} = |\tilde{t}_\mathbf{k}| = \frac{J}{2}[3 + 2\cos k_1 + 2\cos k_2 + 2\cos(k_1 - k_2)]^{1/2}$, with $\tilde{t}_\mathbf{k} = J\sum_\delta t_{\delta;\mathbf{k}}$ and $t_{\delta;\mathbf{k}} = -\frac{i}{2}e^{-i\mathbf{k}\cdot\boldsymbol{\delta}}$. The real part ($g'$) and imaginary part ($g''$) of the function g of the scattering matrix V are given by $g_{m;\mathbf{k}} = (\tilde{t}^*_\mathbf{k}/\epsilon_\mathbf{k})\sum_\delta \Lambda^\delta_m t_{\delta;\mathbf{k}}/\sqrt{N}$.

The evaluation of the self-energy using Eqs. (3) and (4) is straightforward. In that process and due to $c^\dagger_\mathbf{k} = c_{-\mathbf{k}}$, anomalous commutators $\{d_{1,\mathbf{k}}, d_{2,\mathbf{k}'}\} = \delta_{\mathbf{k},-\mathbf{k}'}$ and their corresponding contractions arise, implying also a time evolution $d_{j,\mathbf{k}}(t) = d_{j,\mathbf{k}} e^{\mp i\epsilon_\mathbf{k} t}$ for $j = 1$ and 2, respectively. Thus, the self-energy exhibits particle-hole (ph) and particle-particle (pp) absorption channels, the amplitudes of which are determined via the diagonal and off-diagonal matrix elements of the matrix V. In the $q = 0$ limit, considered here, the ph-channel vanishes. The pp scattering amplitudes acquire simple forms, and all diagonal and off-diagonal self-energies are described by a *single function* $\Sigma(z)$:

$$\boldsymbol{\Sigma}(z) = \begin{pmatrix} a_1 & b \\ b & a_2 \end{pmatrix}\Sigma(z), \quad \Sigma(z) = \frac{1}{N}\sum_\mathbf{k} A^2_\mathbf{k} \frac{1 - 2f_\mathbf{k}}{2\epsilon_\mathbf{k} - z}, \tag{5}$$

for $\omega \gtrless 0$, and $\Sigma'(-\omega) = \Sigma'(\omega)$ and $\Sigma''(-\omega) = -\Sigma''(\omega)$. As usual, we abbreviate $\mathrm{Re}(x) = x'$ and $\mathrm{Im}(x) = x''$. The matrix elements are $a_1 = \Lambda_1(3 + \lambda_1^2)/\Lambda_2$, $a_2 = \Lambda_2(1 - \lambda_2)^2/\Lambda_1$, and $b = \lambda_1(1 - \lambda_2)$; the scattering amplitude is $A_\mathbf{k} = \Lambda_1\Lambda_2 \cos(\sqrt{3}ak_x/2)\sin(3ak_y/2)/(2\epsilon_\mathbf{k})$; and $f_\mathbf{k} = 1/(e^{\epsilon_\mathbf{k}/T} + 1)$ is the Fermi-Dirac distribution. We note that for $\lambda_2 = 1$ the E_{g_2} spin-phonon Hamiltonian satisfies $\mathcal{H}_2 \propto H_K$, leading to no scattering for that mode, and for $\lambda_1 = 0$, symmetry prevents mixing of the E_{g_1} and E_{g_2} modes.

B. Random gauge

For temperatures $T \gtrsim T^*$, thermal gauge excitations need to be taken into account. However, for $T \gtrsim 0.1J \gg T^*$ a random averaging over maximally disordered configurations of $\eta_{\delta_3}(\mathbf{r})$ is sufficient to describe the fermionic system's properties. As this breaks translational invariance, we resort to a numerical real-space evaluation of the defect-averaged self-energy $\boldsymbol{\Sigma}(z)$. This approach has been detailed in Refs. [43,53] and is recapitulated in Appendix B.

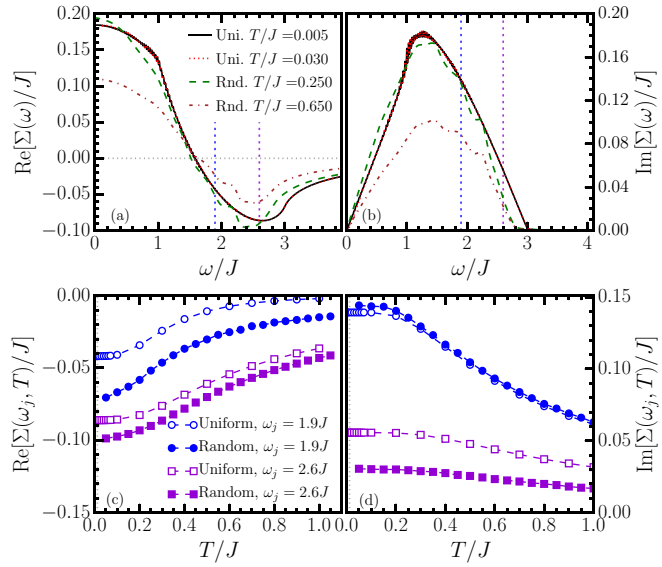

FIG. 2. Panels (a) and (b): Frequency dependence of Σ' and Σ'', respectively, for two temperatures ($T/J = 0.005$ and 0.03) in the uniform gauge field sector, with $L = 200$ (curves overlap), and for two temperatures ($T/J = 0.25$ and 0.65) within random gauge sectors, on lattices of $L = 30$, averaged over $N_R = 200$ maximally disordered configurations. For all cases, $i0^+ = i0.01J$ and $\Lambda_{1,2}/J = 1$. Dashed blue (purple) lines at $\omega_j/J = 1.9$ (2.6) on both panels indicate the position of the phonon modes $E_{g_1}(E_{g_2})$. Panels (c) and (d): Temperature dependence of Σ' and Σ'', respectively, at the phonon frequencies $\omega/J = 1.9$ (blue circles) and $\omega/J = 2.6$ (purple squares). Open (solid) symbols indicate results acquired for uniform (random) gauge field configurations.

C. Results

In Fig. 2, we present results for the self-energy Σ versus frequency and temperature, for both homogeneous and random gauge states. In Figs. 2(a) and 2(b), we plot $\Sigma'(\omega, T)$ and $\Sigma''(\omega, T)$, respectively, obtained from the analytical approach at $T = 0.005J < T^*$ and $T = 0.030J \gtrsim T^*$ (curves overlap) and from the numerical one at $T = 0.25J, 0.65J \gg T^*$. Analytical calculations are performed on lattices with $L = 200$ while numerical ones are performed on lattices with $L = 30$ and averaged over $N_R = 200$ realizations. Both Σ' and Σ'' contribute to the renormalization of the E_{g_1} and E_{g_2} phonons, the energy of which is marked with a blue dotted line and a purple dotted line, respectively. Since $\Sigma'(\omega_j, T) < 0$ at both anticipated phonon energies ω_j, a downward renormalization will occur. Most importantly, however, regarding their lifetime, both phonons reside in a range of negative slope of Σ'' versus ω. Therefore, the lifetime will be dispersive, with phonon spectral functions that display asymmetric line shapes with enhanced left-broadening.

Regarding the gauge excitations, we observe that the overall shape of Σ displays no qualitative change compared to the uniform gauge sector with only some additional fine structure arising from the gauge field excitations. However, there is a reduction of the bandwidth to $<3J$, which affects the

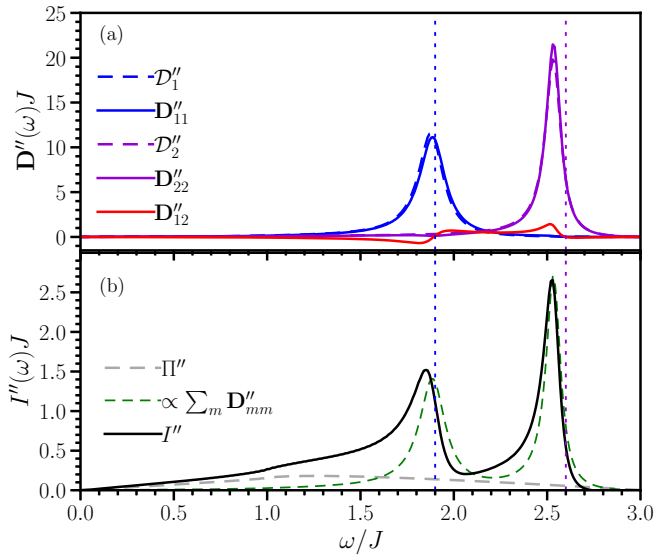

FIG. 3. (a) Frequency dependence of the phonon spectral weight as evaluated via Eqs. (3) and (5) for $\Lambda_{1(2)}/J = 0.3(0.9)$ and $\lambda_{1,2} = 2$. Solid lines represent the elements of the 2×2 phonon propagator $\mathbf{D}''_{mn}$, while dashed lines represent the decoupled phonon modes $\mathcal{D}''_m$. (b) Frequency dependence of the total Raman intensity I'' (black solid line), evaluated via Eq. (6) using the phenomenological parameters $r_m = -0.3$ and $C_m = 0.8J$ and keeping $\mathbf{\Lambda}_m$ as in panel (a). For comparison, the diagonal phonon spectral weight $\sum_m \mathbf{D}''_{mm}(\omega)$ is plotted (green dashed line, rescaled by 1/8 for visual reasons), and the fermionic Raman response, $\sim\Pi''(\omega)$ (gray dashed line), is also plotted. In both panels, Eq. (5) is used with $L = 200$, $T = 0.01J$, and $i0^+ = i0.01J$.

scattering of the high-frequency mode E_{g_2}. Finally, there is a clearly visible reduction of Σ with increasing T. This is dictated by the Fermi-function [as in Eq. (5)] reducing the available phase space. For the low-T results, this effect is too small to be observable.

In Figs. 2(c) and 2(d), we scan the temperature dependence of the real part and the imaginary part of the self-energy, respectively, at the two frequencies of the phonon modes. In doing so, we plot results obtained from both the analytical approach and the numerical approach—even though in principle the former is applied for temperatures beyond its validity. This figure clearly demonstrates that, for the renormalization of optical phonons, gauge field excitations yield only small quantitative corrections. For the rest of the paper, we therefore remain in the uniform gauge configuration.

IV. PHONON PROPAGATORS

Next we discuss the renormalized optical phonon modes, obtained from the 2×2 Dyson equation, Eq. (3), using $\mathbf{\Sigma}$ from Eq. (5). Since a *quantitative* theory for the Majorana-phonon coupling constants is *not* available, we select a set of intermediate values of $\Lambda_1(\Lambda_2) = 0.3J(0.9J)$, $\lambda_{1,2} = 2$, to draw several main conclusions. While these couplings are chosen to roughly mimic existing experiments [46–51], we refrain from attempting to "fit" measured data, since an unjustified fine-tuning could be misleading. The phonon spectra at $T = 0.01J$ and for $L = 200$ are shown in Fig. 3(a). First, and in general, because of $b \neq 0$, phonon mixing by virtue of the fermionic background will occur, i.e., $\mathbf{D}_{mm} \neq [[D^0_m]^{-1} - a_m\Sigma]^{-1} \equiv \mathcal{D}_m$. However, while staying in the perturbative regime, $b\Sigma[(\omega_2 + \omega_1)/2]/(\omega_2 - \omega_1) \ll 1$, the mixing is weak and can be ignored. This is evident from the figure, where $\mathbf{D}''_{12} \ll \mathbf{D}''_{11(22)}$ and $\mathbf{D}''_{mm} \approx \mathcal{D}''_m$, essentially rendering the two phonon modes decoupled. Second, both diagonal elements of $\mathbf{D}$ exhibit the anticipated downward renormalization with respect to ω_m, largest for E_{g_2}. In accordance with Fig. 2(c), the modes' peaks will shift upwards to ω_m as the temperature is increased. Moreover, in accordance with Fig. 2(d), the width of the phonon mode shrinks as the temperature is increased; i.e., in contrast to most conventional excitations in many-body systems, their lifetime grows with temperature.

Finally, one of the most debated features of the phonon modes, as observed in Raman experiments, is their asymmetry, conventionally attributed to the Fano effect [59], i.e., the *interference* of the Majorana continuum with the phonon modes, suggested to reveal the QSL. However, as can be seen from Figs. 3(a) and 3(b), already the individual and the total phonon intensities show a slight asymmetry, due to the frequency dependence of $\Sigma''(\omega)$. While the size of these asymmetries can certainly be fine-tuned by varying the model parameters, the main qualitative point is unavoidable, i.e., that asymmetric phonon lines are *not* the sole consequence of the Fano effect.

V. RAMAN RESPONSE AND FANO LINE SHAPE

Finally, we *speculate* on the Raman cross section $I(z)$. Light scatters from both the lattice *and* the magnetic degrees of freedom. *This* forces the Fano effect to occur [59] and renders the Raman cross section a coupled three-channel problem, with Raman vertices F and $R_{m=1,2}$, encoding the couplings of incoming (outgoing) light fields to the fermions and the two phonon modes, respectively. Presently, only the Loudon-Fleury vertex F is known microscopically [38,39,60], but has been questioned recently [61]. Therefore, obtaining $I(z)$ from first principles is infeasible. To make progress, we resort to *phenomenological* simplifications. These are detailed in Appendix D, but essentially amount to the following. (i) We replace the Raman vertices F and $R_{m=1,2}$ by mere constants, dependent on the scattering geometry. (ii) The three-channel problem comprises additional types of fermionic two-particle propagators contracted with the unknown Raman vertices. We approximate these propagators by $\Sigma(\omega)$, since it mimics the fermionic background (see Appendix D). Comparing Figs. 2(a) and 2(b) with, e.g., the known *magnetic* Raman response [38,39], i.e., the two-particle propagator contracted with $|F|^2$, this seems acceptable. (iii) We ignore phonon mixing, justified by Fig. 3(a). This leads to [Eq. (D4) in Appendix D]

$$I(z) \approx \Pi(z) + \sum_{m=1,2} [r_m + C_m\Pi(z)]^2 \mathbf{D}_{mm}(z), \tag{6}$$

where $\Pi(z) = \Sigma(z)[J/(\Lambda_1\Lambda_2)]^2$ and $I(z)$ is normalized to F, i.e., $I(z) \to I(z)/F^2$, leaving four free parameters, namely, $r_m = R_m/F$ and the coupling constants C_m, which allow us to adjust the strength of the Fano effect. $I(z)$ is a retarded propagator, i.e., its spectrum maps to measurements of a cross

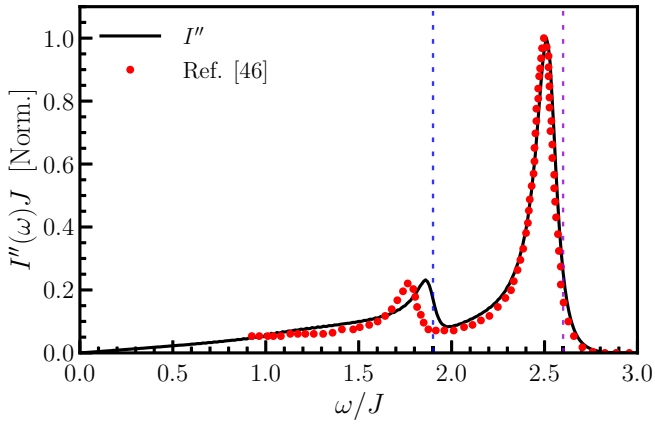

FIG. 4. Comparison of the total Raman intensity I'' (black solid line), evaluated via Eq. (6) for the phenomenological parameters $r_{1(2)} = -0.18(-0.5)$ and $C_{1(2)}/J = 0.65(1)$ with experimental data, taken from Ref. [46] (red points). $L = 200$, $T = 0.01J$, and $i0^+ = i0.01J$ were used for numerical evaluations.

section, which has already been corrected by the fluctuation-dissipation prefactor.

In Fig. 3(b), we plot $I''(\omega)$, for empirically chosen $r_m = -0.3$ and $C_m = 0.8J$, together with $\Pi''(\omega)$, as well as the rescaled diagonal intensity $\sum_m \mathbf{D}''_{mm}(\omega)$ from Fig. 3(a). The overall shape of the Raman response $I''(\omega)$ is clearly different from the diagonal phonon intensity, $\propto \sum_m \mathbf{D}''_{mm}(\omega) \approx \sum_m \mathcal{D}''_m(\omega)$, green dashed line in Fig. 3(b), which would approximate the response if only phonon scattering had been taken into account but not the Fano effect. A broad continuum due to the fractionalized magnetic excitations is visible, on top of which two asymmetric phonon line shapes reside. The optical phonon lines are asymmetrically broadened with characteristic sharp, almost vertical, drop-off only on the high-frequency side of the mode. These features can be traced back to the combination of the asymmetric phonon self-energy, which has its origin in the frequency dependence of the Majorana density of states, on the one hand and to the Fano effect on the other hand.

Finally we compare our theory with experiments [46–50]. The experimental data exhibit a behavior very similar to that of our calculated spectrum, namely, a broad continuum with two asymmetric phonon line shapes. In order to have a direct comparison between theoretical and experimental findings, Fig. 4 displays the Raman spectrum adapted from Ref. [46], along with Eq. (6), employing a set of r's and C's which reproduces the experimental spectrum best. As is evident from this figure, our theory provides a very good description of the experimental data. In fact, the high-energy phonon mode is reproduced almost quantitatively, while only a slight difference appears around the low-frequency phonon mode. The latter could in principle be improved at the expense of additional fine-tuning of the bare ω_{g_1} energy.

VI. SUMMARY AND DISCUSSION

We have developed a microscopic theory for optical phonons, coupled to a Kitaev QSL. This comprises predictions for the impact of the QSL on the frequency renormalization, on the occurrence of an asymmetric line shape, and on the temperature variations. Moreover, we have combined this theory with a phenomenological description of Raman scattering showing that asymmetric line shapes are not driven only by the Fano effect and that experimental data are consistent with our results. Should *ab initio* calculations provide the spin-phonon coupling constants in the future, it would allow for a more accurate and justified theoretical description of the experimental findings [62]. In addition, it is relevant to understand the effect of non-Kitaev additional interactions, either perturbatively (see Ref. [35]) or using J-K-Γ models. Finally, the action of a weak magnetic field is briefly discussed in Appendices A and C, but it needs further theoretical and experimental attention [27,50], especially beyond the weak field limit.

ACKNOWLEDGMENTS

We acknowledge helpful discussions with D. Wulferding, K. Burch, P. Lemmens, S. Bhattacharjee, and R. Moessner. We are grateful to R. Valentí and S. Biswas for clarifications on optical phonons, extracted from *ab initio* methods. The work of A.M. and W.B. has been supported in part by the DFG through Project A02 of SFB 1143 (Project No. 247310070), by Nds. QUANOMET, and by the National Science Foundation under Grant No. NSF PHY-1748958. W.B. also acknowledges the kind hospitality of the PSM, Dresden.

APPENDIX A: MAJORANA-PHONON COUPLING WITH FINITE MAGNETIC FIELD

A magnetic field can be included in the Kitaev spin Hamiltonian according to

$$H_K = \sum_{\mathbf{r}} \sum_{\boldsymbol{\delta}} J_{\delta} S^{d_{\delta}}_{\mathbf{r}} S^{d_{\delta}}_{\mathbf{r}-\boldsymbol{\delta}} + g\mu_B \mathbf{B} \sum_{\mathbf{r}} \mathbf{S}_{\mathbf{r}}. \tag{A1}$$

We repeat here the notation conventions: $\mathbf{r} = l_1\mathbf{a}_1 + l_2\mathbf{a}_2$ runs over one sublattice, with $l_j = 0, 1, \ldots, L-1$, for $j = 1$ and 2, while $\boldsymbol{\delta}$ runs over the three vectors connecting the two sublattices. The number of unit cells is $N = L^2$. The vectors $\boldsymbol{\delta}$ and $\mathbf{a}$ are given by

$$\begin{bmatrix} \boldsymbol{\delta}_1 \\ \boldsymbol{\delta}_2 \\ \boldsymbol{\delta}_3 \end{bmatrix} = \frac{a}{2} \begin{bmatrix} \sqrt{3} & 1 \\ -\sqrt{3} & 1 \\ 0 & -2 \end{bmatrix} \begin{bmatrix} \boldsymbol{e}_x \\ \boldsymbol{e}_y \end{bmatrix},$$
$$\begin{bmatrix} \mathbf{a}_1 \\ \mathbf{a}_2 \\ \mathbf{a}_3 \end{bmatrix} = \frac{a\sqrt{3}}{2} \begin{bmatrix} 2 & 0 \\ 1 & \sqrt{3} \\ -1 & \sqrt{3} \end{bmatrix} \begin{bmatrix} \boldsymbol{e}_x \\ \boldsymbol{e}_y \end{bmatrix}. \tag{A2}$$

Furthermore, the indices d_{δ} of the spin-1/2 operators S acquire the values $d_{\delta} = x$, y, and z depending on the $\boldsymbol{\delta}$ vector of the bond, while the Kitaev interactions J_{δ} are considered to be isotropic. The magnetic field is $\mathbf{B} = (B, B, B)$, while $g = 1$ is the g factor, $\mu_B = 1$ is the Bohr magneton, and we also set to unity the Planck and Boltzmann constants, $\hbar$, $k_B = 1$.

Treating the magnetic field perturbatively for $B < \Delta$ enables a rewriting of Hamiltonian (A1) in terms of the Majorana fermions c and $\tilde{c}$ discussed in the main text [4,63]. In the fermionic representation, the Zeeman term of Eq. (A1)

results in a next-nearest-neighbor (NNN) hopping. Therefore, regarding the spin subsystem, the Hamiltonian H_K reads

$$H_K = H_1 + H_2, \quad H_1 = \sum_{\mathbf{r},\delta} J_\delta h_\delta(\mathbf{r}),$$
$$h_\delta(\mathbf{r}) = -\frac{i}{4}\eta_\delta(\mathbf{r}) c_\mathbf{r}\tilde{c}_{\mathbf{r}-\delta},$$
$$H_2 = -i\frac{\tilde{J}}{8}\sum_{\mathbf{r},\mathbf{a}}[\zeta_\mathbf{a}(\mathbf{r})c_\mathbf{r}c_{\mathbf{r}-\mathbf{a}} + \tilde{\zeta}_\mathbf{a}(\mathbf{r})\tilde{c}_{\mathbf{r}-\delta_3}\tilde{c}_{\mathbf{r}-\delta_3+\mathbf{a}}]. \quad \text{(A3)}$$

H_1 is identical to that in Eq. (1) of the manuscript, with $\eta_{\delta_1}(\mathbf{r}) = \eta_{\delta_2}(\mathbf{r}) = 1$ and $\eta_{\delta_3}(\mathbf{r}) = \pm 1$ corresponding to the $\mathbb{Z}_2$ gauge field arising from the freezing of the $\bar{c}$ species of the Majorana fermions. The tilde on the second Majorana operator is introduced to discriminate between the two sublattices. H_2 follows from the fermionization of a three-spin term which arises within third-order perturbation theory from the spin model. The summation on $\mathbf{a}$ runs over the set of *three* $\mathbf{a}$ vectors described in Eq. (A2). The quantities ζ are given by

$$\zeta_{\mathbf{a}_1}(\mathbf{r}) = 1, \quad \zeta_{\mathbf{a}_2}(\mathbf{r}) = -\eta_{\delta_3}(\mathbf{r}),$$
$$\zeta_{\mathbf{a}_3}(\mathbf{r}) = \eta_{\delta_3}(\mathbf{r}-\mathbf{a}_1), \quad \tilde{\zeta}_{\mathbf{a}_1}(\mathbf{r}) = 1,$$
$$\tilde{\zeta}_{\mathbf{a}_2}(\mathbf{r}) = -\eta_{\delta_3}(\mathbf{r}-\mathbf{a}_1), \quad \tilde{\zeta}_{\mathbf{a}_3}(\mathbf{r}) = \eta_{\delta_3}(\mathbf{r}). \quad \text{(A4)}$$

$\tilde{J}$ refers to the NNN effective three-spin coupling generated by the third-order perturbation theory, $\tilde{J} \sim \frac{B^3}{\Delta^2}$, [4,63]. In order to stay in the perturbative regime, $B \lesssim B^* \approx \Delta$, meaning $\tilde{J} \sim O(10^{-2}J)$. It is important to realize that, although $\tilde{J}/J$ is only of the order of 1%, for real materials this corresponds to relatively strong magnetic fields of up to $B^* \approx 10$ T. As we see here, weak values of the effective NNN coupling term do not affect the high-frequency spectrum where the optical phonon modes lie.

Within the magnetoelastic scheme, lattice modulations in Fourier space,

$$\mathbf{u}_\mathbf{q} = \frac{1}{\sqrt{N}}\sum_\mathbf{r} e^{i\mathbf{q}\cdot\mathbf{r}}\mathbf{u}_\mathbf{r}, \quad \tilde{\mathbf{u}}_\mathbf{q} = \frac{1}{\sqrt{N}}\sum_\mathbf{r} e^{i\mathbf{q}\cdot(\mathbf{r}+\delta_2)}\tilde{\mathbf{u}}_\mathbf{r}, \quad \text{(A5)}$$

are expressed in terms of quantized phonon modes,

$$\mathbf{u}_\mathbf{q} = \sum_m \frac{1}{\sqrt{2M\omega_{m\mathbf{q}}}}\left(\gamma^x_{m\mathbf{q}}\hat{e}_x + \gamma^y_{m\mathbf{q}}\hat{e}_y\right)\ \mathcal{B}_{m\mathbf{q}},$$
$$\tilde{\mathbf{u}}_\mathbf{q} = \sum_m \frac{1}{\sqrt{2M\omega_{m\mathbf{q}}}}\left(\tilde{\gamma}^x_{m\mathbf{q}}\hat{e}_x + \tilde{\gamma}^y_{m\mathbf{q}}\hat{e}_y\right)\ \mathcal{B}_{m\mathbf{q}}. \quad \text{(A6)}$$

The coefficients of the polarization vectors are denoted by γ and $\tilde{\gamma}$ for the two sublattices, respectively; M is of the order of the ruthenium mass; and $\mathcal{B}_{m\mathbf{q}} = b_{m\mathbf{q}} + b^\dagger_{m,-\mathbf{q}}$ comprises the sum of phonon annihilation and creation operators at momentum $\pm\mathbf{q}$ and for polarization mode m, while the energy of the phonon mode is $\omega_{m\mathbf{q}}$. This leads to a coupling of the two subsystems by Eq. (2), i.e.,

$$H_{KP} = \sum_{m\mathbf{q}} \mathcal{B}_{m\mathbf{q}}\mathcal{H}_{m,-\mathbf{q}}, \quad \mathcal{H}_{m\mathbf{q}} = \sum_\delta \Lambda^\delta_{m\mathbf{q}} h_{\delta;\mathbf{q}}, \quad \text{(A7)}$$

where $h_{\delta;\mathbf{q}}$ refers *only* to the nearest-neighbor density, $h_{\delta;\mathbf{q}} = \frac{1}{\sqrt{N}}\sum_\mathbf{r} e^{i\mathbf{q}\cdot\mathbf{r}}h_\delta(\mathbf{r})$, and the finite-momentum couplings are

$$\Lambda^\delta_{m,\mathbf{q}} = \frac{\Lambda^\delta_m}{2}(1 + e^{i\mathbf{q}\cdot\delta}), \quad \Lambda^\delta_m = \Lambda_m[1, -1^m, \lambda_m], \quad \text{(A8)}$$

where $m = 1$ and 2 and λ_m denotes a possible anisotropy between the $\boldsymbol{\delta}_{1,2}$ and $\boldsymbol{\delta}_3$ directions. The phonon propagator reads

$$D^{mm'}_{\mathbf{q}\mathbf{q}'}(z) = \langle\langle \mathcal{B}_{m\mathbf{q}}; \mathcal{B}^\dagger_{m'\mathbf{q}'}\rangle\rangle(z), \quad \text{(A9)}$$

where the double brackets denote the Green's function, which for two operators O_1 and O_2 reads as follows:

$$\langle\langle O_1; O_2\rangle\rangle(\tau) = \langle \mathcal{T}_\tau O_1(\tau)O_2\rangle,$$
$$\langle\langle O_1; O_2\rangle\rangle(i\omega_n) = -\frac{1}{\beta}\int_0^\beta d\tau e^{i\omega_n\tau}\langle\langle O_1; O_2\rangle\rangle(\tau), \quad \text{(A10)}$$

where $\beta = 1/T$ is the inverse temperature, ω_n is the Matsubara frequency, $\omega_n = \frac{2\pi n}{\beta}$ (for bosonic Green's functions), $\mathcal{T}$ denotes the time-ordering operator, and $O(\tau)$ is the operator in the Heisenberg picture $O(\tau) = e^{\tau H}Oe^{-\tau H}$, with H being the (sub)system's Hamiltonian. After an analytical continuation in the frequency range, we express the Green's functions in terms of the complex frequency $z = \omega + i0^+$, i.e., $\langle\langle O_1; O_2\rangle\rangle(i\omega_n) = \langle\langle O_1; O_2\rangle\rangle(z)$, with the imaginary broadening being of the order of $i0^+ = O(0.01J)$. In the absence of scattering from Majorana fermions, the free propagator is diagonal, in both momentum $\mathbf{q}$ and mode index m,

$$\left[D^{mm'}_{\mathbf{q}\mathbf{q}'}(z)\right]_0 = \delta_{\mathbf{q}\mathbf{q}'}\delta_{mm'}D^0_{m\mathbf{q}}(z), \quad D^0_{m\mathbf{q}}(z) = \frac{2\omega_{m\mathbf{q}}}{z^2 - \omega^2_{m\mathbf{q}}}. \quad \text{(A11)}$$

The phonon propagator in the interacting system can be evaluated via Dyson's equation:

$$D^{mm'}_\mathbf{q}(z) = \left[\left[D^0_{m\mathbf{q}}(z)\right]^{-1} - \Sigma^{mm'}_\mathbf{q}(z)\right]^{-1},$$
$$\Sigma^{mm'}_\mathbf{q}(z) = \langle\langle \mathcal{H}_{m\mathbf{q}}; \mathcal{H}^\dagger_{m'\mathbf{q}}\rangle\rangle(z). \quad \text{(A12)}$$

In principle, the self-energy $\Sigma^{mm'}_\mathbf{q}$ is not diagonal in the polarization indexes m, leading to a phonon mixing upon inversion of the right-hand side of the Dyson equation, i.e.,

$$D^{mm}_\mathbf{q}(z) \neq \mathcal{D}^m_\mathbf{q}(z), \quad \mathcal{D}^m_\mathbf{q}(z) = \left[\left[D^0_{m\mathbf{q}}(z)\right]^{-1} - \Sigma^{mm}_\mathbf{q}(z)\right]^{-1}. \quad \text{(A13)}$$

To incorporate the magnetic field and the momentum into the results for the uniform gauge sector $\eta_\delta = 1$, the analytical calculations are adapted accordingly. Hamiltonian (A3) can again be diagonalized by Fourier transformation with $c_\mathbf{k} = \frac{1}{\sqrt{2N}}\sum_\mathbf{r} e^{-i\mathbf{k}\cdot\mathbf{r}}c_\mathbf{r}$, with $\{c_\mathbf{k}, c^\dagger_{\mathbf{k}'}\} = \delta_{\mathbf{k},\mathbf{k}'}$, and similarly for the $\tilde{c}$ operators, where $\mathbf{k} = (k_1 + \frac{\pi}{L})\mathbf{G}_1 + (k_2 + \frac{\pi}{L})\mathbf{G}_2$, $k_j = 2\pi l_j/L$, $\mathbf{G}_1 = \frac{1}{3a}(\sqrt{3}\boldsymbol{e}_x - \boldsymbol{e}_y)$, and $\mathbf{G}_2 = \frac{2}{3a}\boldsymbol{e}_y$. The Hamiltonian in reciprocal space reads

$$H_K = \frac{1}{2}\sum_\mathbf{k}\Psi^\dagger_\mathbf{k}\begin{pmatrix}\epsilon_\mathbf{k} & 0\\ 0 & -\epsilon_\mathbf{k}\end{pmatrix}\Psi_\mathbf{k}, \quad \epsilon_\mathbf{k} = \sqrt{|t_\mathbf{k}|^2 + w^2_\mathbf{k}},$$
$$t_\mathbf{k} = \sum_\delta t_{\delta;\mathbf{k}}, \quad t_{\delta;\mathbf{k}} = -\frac{i}{2}J_\delta e^{-i\mathbf{k}\cdot\delta},$$
$$w_\mathbf{k} = \frac{\tilde{J}}{2}\sum_{j=1}^3(-)^j\sin(\mathbf{k}\cdot\mathbf{a}_j). \quad \text{(A14)}$$

The spinor $\Psi_{\mathbf{k}}^{\dagger} = (d_{1,\mathbf{k}}^{\dagger}, d_{2,\mathbf{k}}^{\dagger})$ comprises the two quasiparticle bands. $h_{\delta;\mathbf{q}}$ from Eq. (A7) is

$$h_{\delta;\mathbf{q}} = \frac{1}{2\sqrt{N}} \sum_{\mathbf{k}} \Psi_{\mathbf{k}-\mathbf{q}}^{\dagger} \tilde{V}_{\delta;\mathbf{k}-\mathbf{q},\mathbf{k}} \Psi_{\mathbf{k}},$$

$$\tilde{V}_{\delta;\mathbf{k}_1,\mathbf{k}_2}^{\mu\nu} = \frac{-1}{4\sqrt{\epsilon_{\mathbf{k}_1}\epsilon_{\mathbf{k}_2}}} [t_{\delta;\mathbf{k}_1}^{*} t_{\mathbf{k}_2} \xi_{\mathbf{k}_1\mathbf{k}_2}^{\mu\nu} + t_{\mathbf{k}_1}^{*} t_{\delta;\mathbf{k}_2} \xi_{\mathbf{k}_2\mathbf{k}_1}^{\nu\mu}],$$

$$\xi_{\mathbf{k}_1\mathbf{k}_2}^{\mu\nu} = (-1)^{\nu} \sqrt{\frac{\epsilon_{\mathbf{k}_1} + (-1)^{\mu} w_{\mathbf{k}_1}}{\epsilon_{\mathbf{k}_2} + (-1)^{\nu} w_{\mathbf{k}_2}}}, \tag{A15}$$

where the indexes take the values $\mu, \nu = 1$ and 2. The diagonal matrix elements of $\tilde{V}$ refer to particle-hole (ph) scattering processes and the off-diagonal matrix elements refer to particle-particle (pp) scattering processes. The former contribute with a relative plus sign in $\tilde{V}$, while the latter contribute with a minus sign. Complex conjugation results in $\tilde{V}_{\delta;\mathbf{k}_1,\mathbf{k}_2}^{\mu\nu *} = \tilde{V}_{\delta;\mathbf{k}_2,\mathbf{k}_1}^{\nu\mu}$, leading to $h_{\delta;\mathbf{q}}^{\dagger} = h_{\delta;-\mathbf{q}}$, which ensures the Hermiticity of H_K and H_{KP}. A straightforward evaluation, using Eqs. (A7), (A9), and (A15) and Ref. [64], yields

$$\Sigma_{\mathbf{q}}^{mm'}(z) = \frac{1}{N} \sum_{\mathbf{k}} \left[V_{\mathbf{k}\mathbf{q}m} V_{\mathbf{k}\mathbf{q}m'}^{\mu\mu *} \mathcal{L}_{\mathbf{k},\mathbf{q}}^{\mathrm{ph}}(z) - V_{\mathbf{k}\mathbf{q}m}^{\mu\bar{\mu}} V_{\mathbf{k}\mathbf{q}m'}^{\mu\bar{\mu} *} \mathcal{L}_{\mathbf{k},\mathbf{q}}^{\mathrm{pp}}(z) \right],$$

$$\mathcal{L}_{\mathbf{k},\mathbf{q}}^{\mathrm{ph}}(z) = \frac{f_{\mathbf{k}+\mathbf{q}} - f_{\mathbf{k}}}{\epsilon_{\mathbf{k}+\mathbf{q}} - \epsilon_{\mathbf{k}} - z} + \frac{f_{\mathbf{k}+\mathbf{q}} - f_{\mathbf{k}}}{\epsilon_{\mathbf{k}+\mathbf{q}} - \epsilon_{\mathbf{k}} + z},$$

$$\mathcal{L}_{\mathbf{k},\mathbf{q}}^{\mathrm{pp}}(z) = \frac{1 - f_{\mathbf{k}+\mathbf{q}} - f_{\mathbf{k}}}{\epsilon_{\mathbf{k}+\mathbf{q}} + \epsilon_{\mathbf{k}} + z} + \frac{1 - f_{\mathbf{k}+\mathbf{q}} - f_{\mathbf{k}}}{\epsilon_{\mathbf{k}+\mathbf{q}} + \epsilon_{\mathbf{k}} - z}. \tag{A16}$$

The scattering amplitude for both contributions is a real number, determined by the matrix $V_{\mathbf{k}\mathbf{q}m} = \sum_{\delta} \Lambda_{\mathbf{q}m}^{\delta} \tilde{V}_{\delta;\mathbf{k}+\mathbf{q},\mathbf{k}}$, while $\mu(\bar{\mu})$ can be chosen as either $\mu = 1(2)$ or $\mu = 2(1)$. The particle-hole $\mathcal{L}_{ij}^{\mathrm{ph}}(z)$ and particle-particle $\mathcal{L}_{ij}^{\mathrm{pp}}(z)$ Lindhard functions set the frequency and temperature dependence, with f_j being the Fermi-Dirac distribution $f_j = 1/(e^{\epsilon_j/T} + 1)$. For $q = 0$, $\mathcal{L}_{\mathbf{k},\mathbf{0}}^{\mathrm{ph}}(z)$ is identically zero and only the pp channel contributes to the self-energy. After some algebra one arrives at Eq. (5) of the manuscript. For $\mathbf{q} \neq 0$ the self-energy cannot be expressed in terms of a single function only.

APPENDIX B: NUMERICAL METHOD FOR DISORDERED GAUGE SECTORS

For temperatures $T \gg T^*$, gauge excitations need to be taken into account. For that, a random averaging over maximally disordered configurations is sufficient to describe the fermionic system's properties [53]. Since translation invariance is broken, we resort to numerical methods in real space, while following the same steps as for the analytical calculation. This means we first set a real-space spinor with the $2N$ Majorana operators, $C^{\dagger} = (c_{\mathbf{r}_1}, \ldots, c_{\mathbf{r}_N}, \tilde{c}_{\mathbf{r}_1-\delta_3}, \ldots, \tilde{c}_{\mathbf{r}_N-\delta_3})$, as the original representation to setup operators, $\hat{O} = C^{\dagger} O C$. Next, we change to a Dirac fermion basis $D = FC$, where $D^{\dagger} = (d_{\mathbf{k}_1}^{\dagger}, \ldots, d_{\mathbf{k}_N}^{\dagger}, d_{\mathbf{k}_1}, \ldots, d_{\mathbf{k}_N})$ and F is the Fourier transform with its matrix elements being defined as $F_{ij} = e^{i\mathbf{k}_i \cdot \mathbf{R}_j}/\sqrt{2N}$, with $\mathbf{R}_j = \mathbf{r}_j$ or $\mathbf{R}_j = \mathbf{r}_j - \boldsymbol{\delta}_3$ for $1 \leqslant j \leqslant N$ or $N+1 \leqslant j \leqslant 2N$, respectively. The last step is to switch to the Hamiltonian's diagonal basis, $E^{\dagger} = (e_1^{\dagger}, \ldots, e_N^{\dagger}, e_1, \ldots, e_N)$, with $E = UD$, where U is a numerical Bogoliubov transformation. The self-energy from Eq. (A12) is then evaluated by writing operators as

$$\hat{O} = E^{\dagger} \tilde{O} E, \quad \text{with} \quad \tilde{O} = U^{\dagger}[(2F^{\dagger}) O (2F)] U, \tag{B1}$$

resulting in an expression similar to Eq. (A16), i.e.,

$$\Sigma_{\mathbf{q}}^{mm'}(z) = 2 \sum_{i,j=1}^{N} \left\{ (\tilde{\mathcal{H}}_{m\mathbf{q}})_{\bar{i}\bar{j}} [(\tilde{\mathcal{H}}_{m'\mathbf{q}}^{\dagger})_{\bar{j}\bar{i}} - (\tilde{\mathcal{H}}_{m'\mathbf{q}}^{\dagger})_{ij}] \mathcal{L}_{ij}^{\mathrm{ph}}(z) + (\tilde{\mathcal{H}}_{m\mathbf{q}})_{i\bar{j}} [(\tilde{\mathcal{H}}_{m'\mathbf{q}}^{\dagger})_{\bar{j}i} + (\tilde{\mathcal{H}}_{m'\mathbf{q}}^{\dagger})_{i\bar{j}}] \mathcal{L}_{ij}^{\mathrm{pp}}(z) \right\}, \tag{B2}$$

where $\bar{i}(\bar{j}) = i + N(j + N)$, $\tilde{\mathcal{H}}$ is dictated by Eqs. (A7) and (B1), and the Lindhard functions are given by

$$\mathcal{L}_{ij}^{\mathrm{ph}}(z) = \frac{f_i - f_j}{\epsilon_i - \epsilon_j + z} + \frac{f_i - f_j}{\epsilon_i - \epsilon_j - z},$$

$$\mathcal{L}_{ij}^{\mathrm{pp}}(z) = \frac{1 - f_i - f_j}{\epsilon_i + \epsilon_j + z} + \frac{1 - f_i - f_j}{\epsilon_i + \epsilon_j - z}, \tag{B3}$$

with ϵ_i being the energy eigenvalues and f_i being the corresponding Fermi-Dirac distribution.

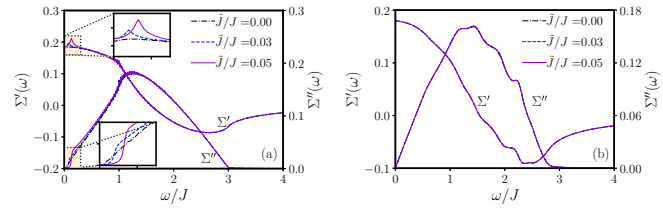

FIG. 5. Phonon self-energy $\Sigma(\omega)$ for various NNN couplings $\bar{J}/J = 0$, 0.03, and 0.05. (a) Within the uniform gauge sector at $T/J = 0.01$ and for $L = 200$. (b) For random gauges, averaging over $N_R = 200$ maximally disordered sectors at $T/J = 0.3$ and $L = 30$.

APPENDIX C: MAGNETIC FIELD DEPENDENCE

In Fig. 5(a), we present results for the effect of the magnetic field on the self-energy $\Sigma(\omega)$ at $\mathbf{q} = 0$. Various values of the NNN coupling $\tilde{J}$ are depicted. This figure clearly demonstrates that the magnetic field is relevant only for low frequencies due to the gap opening. This can be important for acoustic phonons [44]; however, for the optical phonon modes beyond the gap, magnetic fields play no role. In Fig. 5(b), we present numerical results for $\Sigma(\omega)$ obtained numerically after random averaging over $N_R = 200$ maximally disordered sectors on a system with a linear dimension of $L = 30$ and at $T = 0.3J$. Figure 5(b) illustrates that elevated temperatures completely conceal the weak effect of the magnetic field, in the whole frequency range.

The robustness of Σ at higher frequencies against the magnetic field has an important implication regarding the validity of our results in realistic systems. Material realizations of the Kitaev model inevitably host additional magnetic interactions which tend to order the magnetic moments at low temperatures and, therefore, conceal the properties of the quantum spin-liquid (QSL) phase. A common practice in experiments is to destroy the ordering by inducing an in-plane magnetic field and driving the system into the QSL phase. In that respect, our results including the magnetic field show that our calculations are robust against additional magnetic interactions and external magnetic fields. This becomes even more

important, since later we approximate the fermionic Raman response with Σ; namely, we expect that also this will not change under a magnetic field.

APPENDIX D: RAMAN CROSS SECTION

Here we explain the steps which lead to phenomenological Eq. (6) of the main text for the Raman intensities. First we consider the Raman cross section of a fictitious system at momentum zero and energy z, comprising two optical phonons, with *bare* Green's functions $D_{0i=1,2}(z)$, coupled to a fermionic background, with a particle-hole Green's function $\Pi(z)$.

Both phonons and the fermionic background are assumed to be Raman active. We proceed by strongly simplifying all Raman operators F and $R_{i=1,2}$ of the fermionic background and the phonons, as well as the fermion-phonon coupling matrix elements $C_{i=1,2}$, to be real *constants*. Then, to leading order in the fermion-phonon coupling, the total cross section $\propto |\mathrm{Im}[I(\omega + i0^+)]|$ derives from a trace over the Dyson equation (apart from the trivial fluctuation-dissipation prefactor):

$$I(z) = \begin{bmatrix} F \\ R_1 \\ R_2 \end{bmatrix}^{\dagger} \left[\mathbb{G}_0^{-1}(z) - \mathbb{V}\right]^{-1} \begin{bmatrix} F \\ R_1 \\ R_2 \end{bmatrix},$$
$$\mathbb{G}_0(z) = \begin{bmatrix} \Pi(z) & 0 & 0 \\ 0 & D_{01}(z) & 0 \\ 0 & 0 & D_{02}(z) \end{bmatrix}, \qquad \text{(D1)}$$
$$\mathbb{V} = \begin{bmatrix} 0 & C_1 & C_2 \\ C_1 & 0 & 0 \\ C_2 & 0 & 0 \end{bmatrix}.$$

This can be written differently as

$$I(z) = \Pi(z) + \begin{bmatrix} r_1 + \Pi(z)C_1 \\ r_2 + \Pi(z)C_2 \end{bmatrix}^T \mathbb{D}(z) \begin{bmatrix} r_1 + C_1\Pi(z) \\ r_2 + C_2\Pi(z) \end{bmatrix}, \qquad \text{(D2)}$$

where $\mathbb{D}(z)$ is the *dressed* 2×2 phonon Green's function,

$$\mathbb{D}(z) = \left[\mathbb{D}_0^{-1}(z) - \begin{bmatrix} C_1^2 & C_1C_2 \\ C_1C_2 & C_2^2 \end{bmatrix} \Pi(z)\right]^{-1}, \qquad \text{(D3)}$$

with $\mathbb{D}_0(z)$ being the lower 2×2 block of $\mathbb{G}_0(z)$. Henceforth, we normalize $r_i = R_i/F$, and $I(z)/F^2 \to I(z)$. That is, F is set to unity. Equation (D2) can either be derived by simple algebra from Eq. (D1) or be visualized by iterating the corresponding diagrams. The latter is shown in Fig. 6. Note that all entries of Eq. (D2), i.e., $\propto F^2$, $\propto R^2$, and $\propto FR$, are infinite-order series of RPA type, as can be read off from Fig. 6. Any additional renormalizations of the Majorana particles, e.g., by phonon self-energies, or of the phonons by anharmonicities, are higher-order effects and would require vertex corrections to be incorporated in all three channels of Eq. (S26) by virtue the Kadanoff-Baym scheme and vice versa. This is beyond our study.

Several comments regarding Eq. (D2) are in order. First, contributions of type $\Pi(z)C_i\mathbb{D}_{ij}(z)r_j$, Figs. 6(c) and 6(d), from the second addend on its right-hand side represent interference effects between the phononic and the fermionic Raman scattering, i.e., the *Fano effect*. Second, the Fano effect is

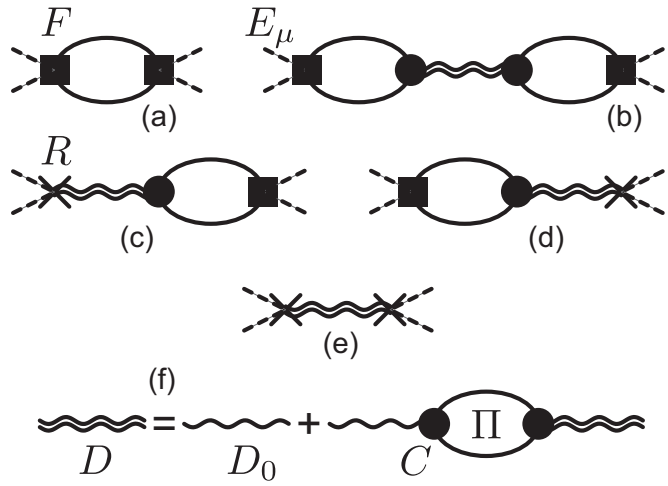

FIG. 6. (a)–(e) Diagrams contributing to the Raman cross section, Eq. (D2). Dashed line: photons. E_μ: electric field. Solid square F, cross R, and solid circle C: Raman and fermion-phonon vertices. Solid steady line: fermions with ellipse Π particle-hole Green's function. (f) Dyson equation, Eq. (D3), for single (double) wiggly line: bare (dressed) phonon Green's function, $\mathbb{D}_0$ ($\mathbb{D}$).

intrinsically tied to the renormalization of the bare phonon by the fermions. Speaking differently, for any $C_{1,2} \neq 0$ and for a finite fermionic and phononic Raman vertex $r_{1,2}^{-1} \neq 0$, the Fano effect is unavoidable. Third, for the problem formulated, the Fano effect is always *complete*. That is, irrespective of the particular form of $\Pi(z)$ and the parameters $C_{1,2}$ and $r_{1,2}$, each phonon gives rise to one energy at which the cross section is *strictly zero*. Fourth, and as a direct consequence of the latter, the causality of the cross section is delicate. For example, simplifying $\mathbb{D}(z)$ in Eq. (D3) by discarding the off-diagonal self-energy, in order to decouple the two phonons, will inevitably lead to regimes of parameters $C_{1,2}$ for which the cross section turns *negative* over certain ranges of ω. This has to be kept in mind when performing additional simplifications.

Turning to the coupled phonon-Majorana system of the present work, evaluating the diagrams of Fig. 6 from first principles is infeasible. This is because they involve momentum summations over unknown form factors which are contained in F *and* R_i and actually turn Eq. (D1) into an integral equation. For the former, i.e., F, the Loudon-Fleury vertex is a conventional choice [38,39,60]. This, however, is open to debate [61]. For the latter, i.e., R_i, derivatives of the dielectric tensor with respect to the normal coordinates need to be used. These are unknown for any putative/proximate Kitaev QSL system. In addition to that the amplitudes of F and R_i are modulated by the scattering geometry. In this situation, and to make progress, we assume four *phenomenological* simplifications for our system. (i) We remain with mere constants for F and R_i. These will differ for different scattering geometries. (ii) The constants $C_{1,2}$, displayed in Eq. (D2) are used as free parameters, independent of $\mathbb{D}(z)$, in order to adjust the magnitude of the Fano effect. (iii) Hereafter, we replace $\mathbb{D}(z)$ with the phonon propagator evaluated in the main text, i.e., $\mathbf{D}(z)$, and we approximate it to be diagonal. (iv) Most important, since the spectrum of the purely magnetic Raman

cross section of Refs. [38,39,60] is very similar in shape to the spectrum of the normalized part of phonon self-energy $\mathrm{Im}\Sigma(\omega + i0^+)$, we approximate $\Pi(z) \approx \Sigma(z)[J/(\Lambda_1\Lambda_2)]^2$ on the right-hand side of Eq. (D1). This is motivated by realizing that the Loudon-Fleury (LF) Hamiltonian describing the coupling of light, with an incoming polarization vector $\boldsymbol{\epsilon}_{\mathrm{in}}$ and an outgoing polarization vector $\boldsymbol{\epsilon}_{\mathrm{out}}$, reads $H_{\mathrm{LF}} = \sum_{\mathbf{r},\boldsymbol{\delta}} J^{d_{\boldsymbol{\delta}}}(\boldsymbol{\epsilon}_{\mathrm{in}} \cdot \boldsymbol{\delta})(\boldsymbol{\epsilon}_{\mathrm{out}} \cdot \boldsymbol{\delta}) S^{d_{\boldsymbol{\delta}}}_{\mathbf{r}} S^{d_{\boldsymbol{\delta}}}_{\mathbf{r}-\boldsymbol{\delta}}$, which is of a form identical to that of the operator $\mathcal{H}_m$ for the magnetoelastic coupling. Altogether one obtains

$$I(z) \approx \Pi(z) + \sum_{m=1,2} [r_m + C_m \Pi(z)]^2 \mathbf{D}_{mm}(z), \tag{D4}$$

which is Eq. (6) of the main text.

For completeness, we emphasize, that $I''(z)$ corresponds to the spectrum of a Green's function. By conventional terminology, this corresponds to the cross section, corrected for by the standard Bose factor of the fluctuation-dissipation theorem.

[1] L. Savary and L. Balents, Rep. Prog. Phys. **80**, 016502 (2017).
[2] Y. Zhou, K. Kanoda, and T.-K. Ng, Rev. Mod. Phys. **89**, 025003 (2017).
[3] J. Knolle and R. Moessner, Annu. Rev. Condens. Matter Phys. **10**, 451 (2019).
[4] A. Kitaev, Ann. Phys. **321**, 2 (2006).
[5] R. Steinigeweg and W. Brenig, Phys. Rev. B **93**, 214425 (2016).
[6] X.-Y. Feng, G.-M. Zhang, and T. Xiang, Phys. Rev. Lett. **98**, 087204 (2007).
[7] N. Wu, Phys. Lett. A **376**, 3530 (2012).
[8] A. Metavitsiadis and W. Brenig, Phys. Rev. B **96**, 041115(R) (2017).
[9] A. Metavitsiadis, C. Psaroudaki, and W. Brenig, Phys. Rev. B **99**, 205129 (2019).
[10] C. E. Agrapidis, J. van den Brink, and S. Nishimoto, Phys. Rev. B **99**, 224418 (2019).
[11] A. Metavitsiadis and W. Brenig, Phys. Rev. B **103**, 195102 (2021).
[12] S. Yang, D. L. Zhou, and C. P. Sun, Phys. Rev. B **76**, 180404(R) (2007)
[13] J. Nasu, M. Udagawa, and Y. Motome, Phys. Rev. Lett. **113**, 197205 (2014).
[14] K. O'Brien, M. Hermanns, and S. Trebst, Phys. Rev. B **93**, 085101 (2016).
[15] P. A. Mishchenko, Y. Kato, and Y. Motome, Phys. Rev. B **96**, 125124 (2017).
[16] G. Baskaran, D. Sen, and R. Shankar, Phys. Rev. B **78**, 115116 (2008).
[17] I. Rousochatzakis, Y. Sizyuk, and N. B. Perkins, Nat. Commun. **9**, 1575 (2018).
[18] P. P. Stavropoulos, D. Pereira, and H.-Y. Kee, Phys. Rev. Lett. **123**, 037203 (2019).
[19] G. Khaliullin, Prog. Theor. Phys. Suppl. **160**, 155 (2005).
[20] G. Jackeli and G. Khaliullin, Phys. Rev. Lett. **102**, 017205 (2009).
[21] J. Chaloupka, G. Jackeli, and G. Khaliullin, Phys. Rev. Lett. **105**, 027204 (2010).
[22] Z. Nussinov and J. van den Brink, Rev. Mod. Phys. **87**, 1 (2015).
[23] S. Trebst, Kitaev materials, in *Topological Matter - Topological Insulators, Skyrmions and Majoranas*, edited by S. Blügel, Y. Mokrousov, T. Schäpers, and Y. Ando, Lecture Notes of the 48th IFF Spring School 2017 (Forschungszentrum Jülich, Jülich, Germany, 2017), Chap. D3, pp. 769–807.
[24] S. M. Winter, A. A. Tsirlin, M. Daghofer, J. van den Brink, Y. Singh, P. Gegenwart, and R. Valentí, J. Phys.: Condens. Matter **29**, 493002 (2017).
[25] M. Hermanns, I. Kimchi, and J. Knolle, Annu. Rev. Condens. Matter Phys. **9**, 17 (2018).
[26] Y. Motome and J. Nasu, J. Phys. Soc. Jpn. **89**, 012002 (2020).
[27] Y. Kasahara, T. Ohnishi, Y. Mizukami, O. Tanaka, S. Ma, K. Sugii, N. Kurita, H. Tanaka, J. Nasu, Y. Motome, T. Shibauchi, and Y. Matsuda, Nature (London) **559**, 227 (2018).
[28] T. Yokoi, S. Ma, Y. Kasahara, S. Kasahara, T. Shibauchi, N. Kurita, H. Tanaka, J. Nasu, Y. Motome, C. Hickey, S. Trebst, and Y. Matsuda, Science **373**, 568 (2021).
[29] O. Tanaka, Y. Mizukami, R. Harasawa, K. Hashimoto, K. Hwang, N. Kurita, H. Tanaka, S. Fujimoto, Y. Matsuda, E.-G. Moon, and T. Shibauchi, Nat. Phys. **18**, 429 (2022).
[30] A. Banerjee, C. A. Bridges, J. Q. Yan, A. A. Aczel, L. Li, M. B. Stone, G. E. Granroth, M. D. Lumsden, Y. Yiu, J. Knolle, S. Bhattacharjee, D. L. Kovrizhin, R. Moessner, D. A. Tennant, D. G. Mandrus, and S. E. Nagler, Nat. Mater. **15**, 733 (2016).
[31] A. Banerjee, J. Yan, J. Knolle, C. A. Bridges, M. B. Stone, M. D. Lumsden, D. G. Mandrus, D. A. Tennant, R. Moessner, and S. E. Nagler, Science **356**, 6342 (2017).
[32] A. Banerjee, P. Lampen-Kelley, J. Knolle, C. Balz, A. A. Aczel, B. Winn, Y. Liu, D. Pajerowski, J. Yan, C. A. Bridges, A. T. Savici, B. C. Chakoumakos, M. D. Lumsden, D. A. Tennant, R. Moessner, D. G. Mandrus, and S. E. Nagler, Nat. Part. J. Quantum Mater. **3**, 8 (2018).
[33] J. Knolle, D. L. Kovrizhin, J. T. Chalker, and R. Moessner, Phys. Rev. Lett. **112**, 207203 (2014).
[34] A. Smith, J. Knolle, D. L. Kovrizhin, J. T. Chalker, and R. Moessner, Phys. Rev. B **92**, 180408(R) (2015).
[35] J. Knolle, S. Bhattacharjee, and R. Moessner, Phys. Rev. B **97**, 134432 (2018).
[36] S.-H. Baek, S.-H. Do, K. Y. Choi, Y.S. Kwon, A.U.B. Wolter, S. Nishimoto, J. van den Brink, and B. Büchner, Phys. Rev. Lett. **119**, 037201 (2017).
[37] J. Zheng, K. Ran, T. Li, J. Wang, P. Wang, B. Liu, Z.-X. Liu, B. Normand, J. Wen, and W. Yu, Phys. Rev. Lett. **119**, 227208 (2017).
[38] J. Knolle, G.-W. Chern, D. L. Kovrizhin, R. Moessner, and N. B. Perkins, Phys. Rev. Lett. **113**, 187201 (2014).
[39] J. Nasu, J. Knolle, D. L. Kovrizhin, Y. Motome, and R. Moessner, Nat. Phys. **12**, 912 (2016).
[40] B. Perreault, J. Knolle, N. B. Perkins, and F. J. Burnell, Phys. Rev. B **92**, 094439 (2015).
[41] Y. Vinkler-Aviv and A. Rosch, Phys. Rev. X **8**, 031032 (2018).
[42] M. Ye, G. B. Halász, L. Savary, and L. Balents, Phys. Rev. Lett. **121**, 147201 (2018).

[43] A. Metavitsiadis and W. Brenig, Phys. Rev. B **101**, 035103 (2020).
[44] M. Ye, R. M. Fernandes, and N. B. Perkins, Phys. Rev. Research **2**, 033180 (2020).
[45] H. Li, T. T. Zhang, A. Said, G. Fabbris, D. G. Mazzone, J. Q. Yan, D. Mandrus, G. B. Halász, S. Okamoto, S. Murakami, M. P. M. Dean, H. N. Lee, and H. Miao, Nat. Commun. **12**, 3513 (2021).
[46] L. J. Sandilands, Y. Tian, K. W. Plumb, Y.-J. Kim, and K. S. Burch, Phys. Rev. Lett. **114**, 147201 (2015).
[47] A. Glamazda, P. Lemmens, S.-H. Do, Y. S. Kwon, and K.-Y. Choi, Phys. Rev. B **95**, 174429 (2017).
[48] T. T. Mai, A. McCreary, P. Lampen-Kelley, N. Butch, J. R. Simpson, J.-Q. Yan, S. E. Nagler, D. Mandrus, A. R. Hight Walker, and R. V. Aguilar, Phys. Rev. B **100**, 134419 (2019).
[49] D. Lin, K. Ran, H. Zheng, J. Xu, L. Gao, J. Wen, S.-L. Yu, J.-X. Li, and X. Xi, Phys. Rev. B **101**, 045419 (2020).
[50] D. Wulferding, Y. Choi, S.-H. Do, C. H. Lee, P. Lemmens, C. Faugeras, Y. Gallais, and K.-Y. Choi, Nat. Commun. **11**, 1603 (2020).
[51] Y. Wang, G. B. Osterhoudt, Y. Tian, P. Lampen-Kelley, A. Banerjee, T. Goldstein, J. Yan, J. Knolle, H. Ji, R. J. Cava *et al.*, npj Quantum Mater. **5**, 14 (2020).
[52] G. Baskaran, S. Mandal, and R. Shankar, Phys. Rev. Lett. **98**, 247201 (2007).
[53] A. Metavitsiadis, A. Pidatella, and W. Brenig, Phys. Rev. B **96**, 205121 (2017).
[54] A. Pidatella, A. Metavitsiadis, and W. Brenig, Phys. Rev. B **99**, 075141 (2019).
[55] See Supplemental Material at http://link.aps.org/supplemental/10.1103/PhysRevB.105.165151 for effect of distortions on models for Kitaev materials.
[56] J. G. Rau, E. K.-H. Lee, and H.-Y. Kee, Phys. Rev. Lett. **112**, 077204 (2014).
[57] W. M. H. Natori, R. Moessner, and J. Knolle, Phys. Rev. B **100**, 144403 (2019).
[58] K. I. Kugel and D. I. Khomskii, Sov. Phys. Usp. **25**, 231 (1982).
[59] U. Fano, Phys. Rev. **124**, 1866 (1961).
[60] P. A. Fleury and R. Loudon, Phys. Rev. **166**, 514 (1968).
[61] Y. Yang, M. Li, I. Rousochatzakis, and N. B. Perkins, Phys. Rev. B **104**, 144412 (2021).
[62] D. A. S. Kaib, S. Biswas, K. Riedl, S. M. Winter, and R. Valentí, Phys. Rev. B **103**, L140402 (2021).
[63] Y.-Z. You, I. Kimchi, and A. Vishwanath, Phys. Rev. B **86**, 085145 (2012).
[64] To arrive at the analytical expression for the self-energy we have also used the useful properties for $\tilde{V}$: $\tilde{V}^{\mu\nu}_{\mathbf{k}_1,\mathbf{k}_2} = -\tilde{V}^{\bar{\mu}\bar{\nu}}_{\mathbf{k}_1,\mathbf{k}_2}$, with $\bar{\mu} = \mu - (-1)^{\mu}$, and $\tilde{V}^{\mu\nu}_{-\mathbf{k}_1,-\mathbf{k}_2} = -\tilde{V}^{\bar{\nu}\bar{\mu}}_{\mathbf{k}_2,\mathbf{k}_1}$, where we have dropped the $\boldsymbol{\delta}$ index for simplicity.